

Reconfigurable Shape-Morphing Dielectric Elastomers Using Spatially Varying Electric Fields

Ehsan Hajiesmaili¹ and David R. Clarke^{1*}

¹Harvard John A. Paulson School of Engineering and Applied Sciences, Cambridge, MA 02138, USA.

Exceptionally large strains can be produced in soft elastomers by the application of an electric field and the strains can be exploited for a variety of novel actuators, such as tunable lenses and tactile actuators. However, shape morphing with dielectric elastomers has not been possible since no generalizable method for changing their Gaussian curvature has been devised. It is shown that this fundamental limitation can be lifted by introducing internal, spatially varying electric fields through a layer-by-layer fabrication method incorporating shaped, carbon-nanotubes-based electrodes between thin elastomer sheets. To illustrate the potential of the method, voltage-tunable negative and positive Gaussian curvatures shapes are produced. Furthermore, by applying voltages to different sets of internal electrodes, the shapes can be re-configured. All the shape changes are reversible when the voltage is removed.

The natural world abounds with shapes that morph as they grow, ranging from the evolution of ripples on leaves¹ to the complex folding of the human brain². As their shapes change, geometrically their Gaussian curvature changes and, as understood from Gauss's theorema egregium, this is only possible because the deformations are spatially inhomogeneous³. Bending,

homogenous expansion, or homogeneous contraction do not change the Gaussian curvature, defined as $\kappa = \kappa_1 \kappa_2 = \frac{1}{r_1 r_2}$, where κ_1 and κ_2 are the principal curvatures of the surface and r_1 and r_2 are radii of curvature. Therefore, under these deformations a body will not be able to morph from one shape to a fundamentally different one. To create spatially inhomogeneous deformations, gradients in deformation are required. One such mechanism that can give rise to shape changes is differential swelling⁴⁻⁷. A second mechanism is inhomogeneous stiffness⁸⁻¹¹. A third mechanism is domain wall motion in magnetostrictive and ferroelastic materials¹².

In this work, morphing of an initially flat elastomer sheet into shapes of different Gaussian curvature is demonstrated based on introducing inhomogeneous internal deformations by creating spatially distributed electric fields. In contrast to the natural world, the shape changes are reversible when the applied voltages are removed. Furthermore, by altering the internal electric field distributions, the shape can be re-configurable. Also, in contrast to other mechanisms for creating shape changes, the changes are not driven by temperature changes or diffusion of species or solutes and so are faster and amenable to electrical control and programming.

Currently, actuators based on dielectric elastomers cannot morph in shape. They are based on what might be termed a compliant capacitor model: a voltage applied to electrodes on opposite sides of a dielectric sheet create opposite net charges. The Coulombic attraction between them produces a stress, the Maxwell stress, in the electric field direction that acts to thin the dielectric. For very soft and incompressible materials, such as elastomers, the Maxwell stress induced thinning is compensated by expansion in the plane of the elastomer. These expansion strains can be large and used to drive an actuator¹³. However, the electric field remains homogeneous

everywhere within the elastomer sheet and consequently, even though the elastomer is compliant, it cannot morph to a new shape; a flat sheet remains flat. Actuators based on the compliant capacitor model either provide in-plane expansion¹³, linear actuation^{14,15}, or bending¹⁶.

To morph, according to Gauss's theorem egregium, a change of intrinsic curvature can only occur when the deformation is spatially inhomogeneous along the surface. In dielectric elastomers, this can be achieved by creating inhomogeneous electric fields when a voltage is applied. As will be shown, this can be accomplished by creating a multilayer structure consisting of a set of dielectric elastomer layers separated by compliant inter-digitated electrodes of different shapes. The meso-architecture of the internal electrodes defines the attainable shapes when voltages are applied. In contrast to elastomers with inhomogeneous stiffness, elastomer sheets with spatially varying internal electric field can be re-configured from one shape to another, by addressing different sets of electrodes.

The shape morphing mechanism is illustrated in Fig. 1. It shows a stack of very thin circular, inter-digitated electrodes separated by thicker layers of circular elastomer sheets. The electrode diameters decrease from bottom to top. Upon applying a voltage between the ground and high-voltage electrodes, shown in grey and red in Fig. 1a, an electric field is induced inside the elastomer layers primarily in those regions where the two adjacent electrodes overlap (active regions, shown in red in Fig. 1b); everywhere outside of these local regions, the electric field is negligible (passive regions, shown in blue in Fig. 1b). The electric field induced deformation consists of a radial expansion of the elastomer between the overlapped electrode segments and a decrease in their spacing, which leads to a differential actuation: greater lateral expansion in the center of the elastomer sheet and decreasing towards the edge (shown by the thickness of the

arrows in Fig. 1c), as well as greater expansion below the midsurface. To accommodate the incompatible strain, the flat disk of elastomer morphs into a shape with positive Gaussian curvature, as shown in Fig. 1d using numerical simulations. The Gaussian curvature is a function of the applied voltage, position along the surface, and design of the electrodes.

Therefore, by designing the electrodes' geometry, one can define the active region within the elastomer sheet which determines both the metric tensor^{4,17} of the surface and applied bending moment. To create relatively simple shapes, as will be described, the appropriate electrode meso-architecture can be identified by a simple intuition and physical arguments aided by numerical analysis of actuation shape (the forward problem). More generally designing the meso-architecture of the electrodes, namely their geometry and arrangement, the spatial position of the actuating regions inside the elastomer and the differential actuation can be defined. More complex morphing shapes will require solution of the inverse problem.

To test the shape-morphing concepts, dielectric elastomers were fabricated in a manner similar to those used for the manufacture of multilayer dielectric elastomer actuators¹⁸. Briefly, as described in greater detail in Methods, a mixture of acrylic oligomers, cross-linkers and photo-initiator was spun coat onto a non-adhesive substrate and then UV cured in place. A mat of electrically percolating carbon nanotubes was then stamped through a mask, defining the shape and size of the electrode, onto the elastomer. Next, the mask was removed and the procedure repeated with different masks to produce the desired number of layers and the electrode meso-architecture. Finally, contacts were made to the individual electrode layers for actuation.

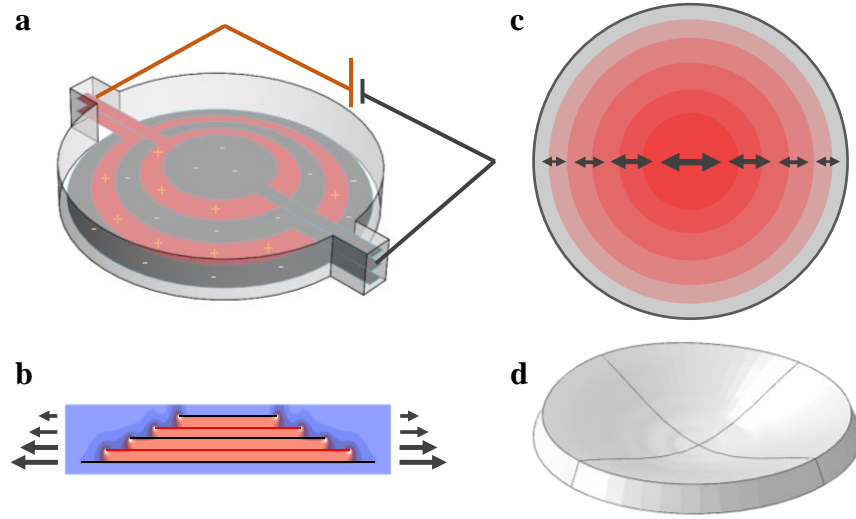


Fig. 1. A generalizable method for shape morphing of thin sheets of elastomer by creating spatially varying internal electric field **(a)** A multilayered structure of circular elastomer sheets interleaved with concentric, inter-digitated electrodes of decreasing radii with height. **(b)** The electric field is primarily concentrated in the regions of overlap between the adjacent electrodes as illustrated by the computed electric field distribution shown in orange. **(c)** Applying a voltage to the electrodes creates a radial actuation strain that varies with both radial position (represented by the length of arrows), and also with vertical position as shown by arrows in **(b)**. **(d)** In response, the circular disk deforms with a positive Gaussian curvature (simulation) that increases with increasing voltage.

To complement the experimental demonstrations, as well as to aid in the design of the electrode meso-architectures, the actuated shapes as a function of applied voltage were computed using a fully coupled electro-mechanical finite elements analysis. The computations followed a standard finite element formulation procedure, in which the governing partial differential equations are

approximated by a system of nonlinear algebraic equations and the resulting system of nonlinear equations solved using Newton-Raphson's iterative method (see the Methods for more details). For the mechanical constitutive equation, a neo-Hookean model¹⁹ was used with a shear modulus of 312 kPa and Poisson ratio of 0.495 (nearly incompressible), based on measurements of the mechanical deformation response of the elastomer used (see Methods for more details). The electrical constitutive equation is defined by a linear relation between the electric displacement and electric field with the relative permittivity of 5.5. Fig. 2 compares the measured profile of a positive curvature dome with increasing electric field with the full electro-mechanically coupled simulations.

To realize shape morphing to a positive Gaussian curvature, an axisymmetric multilayer disk was fabricated consisting of 12 elastomer layers sandwiching 11 circular electrodes whose radii decrease linearly from 11 mm on the top layer to 1 mm on the bottom layer. The resulting meso-architecture is characterized by the number of active regions decreasing with radius, shown with the color intensity in Fig. 2a, but increasing linearly (in steps) with height through the thickness of the elastomer. Applying a voltage produces a differential actuation strain that decreases with radius and increases with height, and therefore the elastomer morphs into a dome shape, as predicted through the numerical analysis Fig. 2b. Photographs and quantification of the shape change as a function of voltage, using a laser sheet light scanner, is presented in Fig. 2c, together with the Gaussian curvature computed from the heights at the indicated voltages. Realtime video recording of actuation of the thin sheet of elastomer into a dome shape is shown in Supplementary Video 1. The measured height profiles as a function of voltage are compared with the predictions of the coupled electro-mechanical analysis in Fig. 2c. Excellent agreement

is found including with the center height as a function of voltage. It is also noteworthy that not only are the strains large, but the displacements can also be large, millimeters.

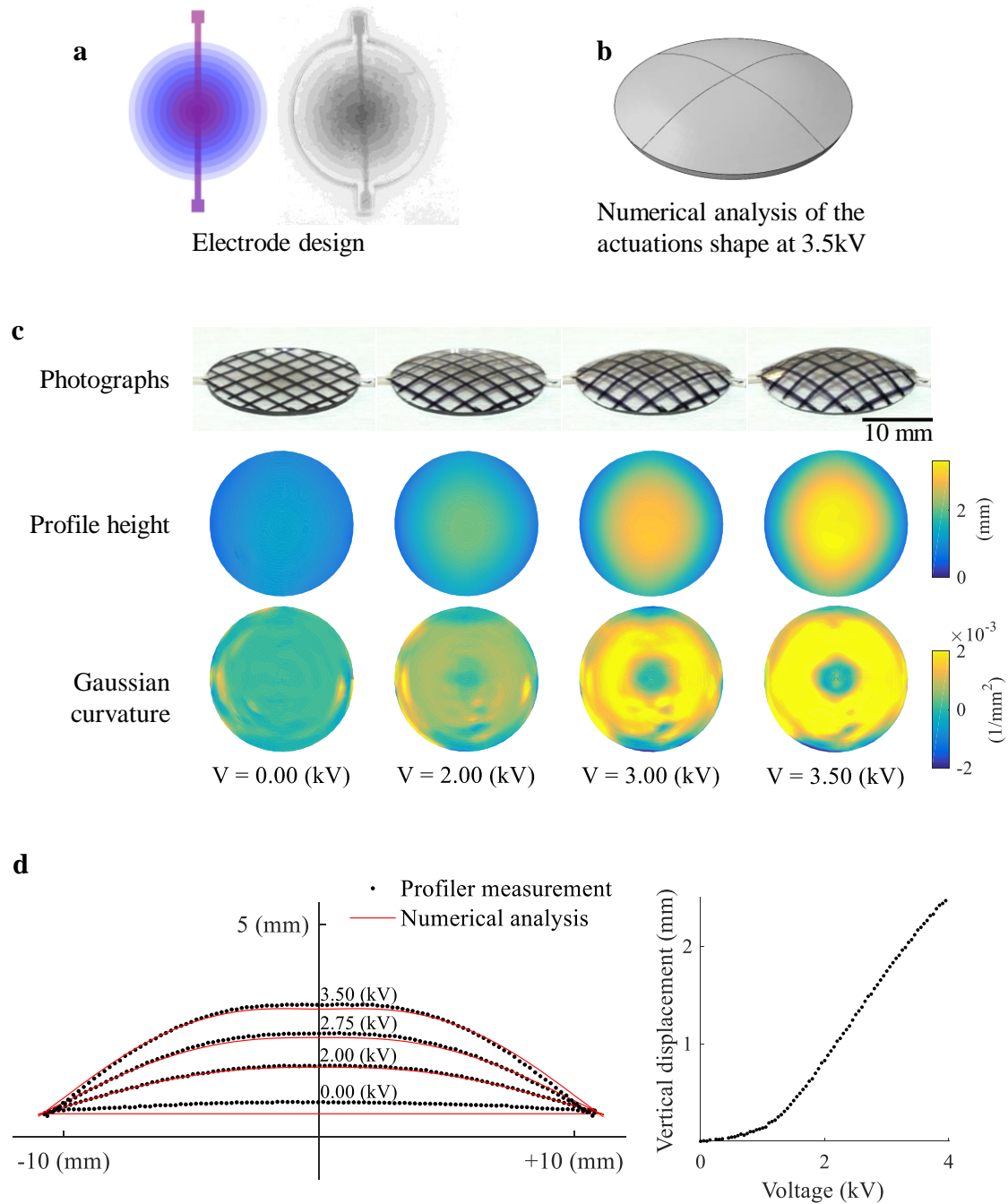


Fig. 2. A thin sheet of dielectric elastomer morphing into a dome shape with positive Gaussian curvature. **(a)** The electrodes are designed such that the number of active regions decreases with the radius (shown schematically with color intensity on the left and a photograph on the right). **(b)** Numerical analysis of this structure shows that the thin sheet of elastomer with such electrode meso-architecture morphs into a dome, when a voltage is applied. **(c)** A series of photographs of the actuation shape at increasing voltages, together with the line scanner profile measurement data and the derived Gaussian curvature shows that the thin sheet of elastomer morphs into a dome with positive Gaussian curvature, increasing with the applied voltage. The elastomers are transparent and so a fiducial grid of black lines was marked on their surface for visualization. **(d)** Comparing the simulation results and profiler measurement for the cross-section of the actuation profile at different voltages (left) and the vertical displacement of the center of the disk as a function of the applied voltage (right) shows excellent agreement between the two.

Changing the meso-architecture of the electrodes changes the Gaussian curvature produced when a voltage is applied. For instance, a thin flat disk of dielectric elastomer morphs into a saddle-like shape with negative Gaussian curvature when the actuation strain increases with radial position through the thickness of the elastomer. Such a strain field can be readily produced in a multilayer dielectric elastomer. In Fig. 3 this was accomplished using 11 circular electrodes sandwiched between 12 elastomer layers. The electrodes were arranged so that their overlap increases linearly with radius, and with the additional feature that on two opposite quadrants of the disk it increases with height while on the other two quadrants it decreases. This electrode configuration

is represented by the blue and red color in the projected electrode density, Fig. 3a. Design of each individual electrode is shown in Extended Data Fig. 3. Applying a voltage produces a strain field that increases radially, bending the elastomer sheet inwards on two opposite quadrants, and outwards on the other two opposite quadrants, resulting in a saddle actuation shape with negative Gaussian curvature, as predicted through numerical analysis (Fig. 3b) and shown in experiment (Fig. 3c). The negative curvature increases with increasing voltage and when the voltage is removed the disk returns to its initial flat shape. Realtime video recording of actuation of the thin sheet of elastomer into a saddle shape is shown in the Supplementary Video 2.

A third simple example is a strip that can morph into a torus segment with positive curvature (the outer part of a torus) , Fig. 3d, or negative curvature (inner part of a torus), Fig. 3e. The number of elastomer and electrode layers was the same as in the previous examples, but both the electrodes and elastomer layers were rectangular and the same length (60 mm). The electric field induced curvature arises from the variation in width of the electrodes. For the torus segment with positive curvature on the left in Fig. 3d, the electrode width decreases from 11 mm on the bottom layer to 1 mm on the top layer. For the right one in Fig. 3d, the electrode width decreases from 22 mm to 2 mm. For the torus segment with negative curvature, Fig. 3e, the electrode on each layer consists of two rectangles of length 60 mm placed at the two edges of the elastomer sheet and their width increases from 11 mm on the bottom layer to 1 mm on the top layer.

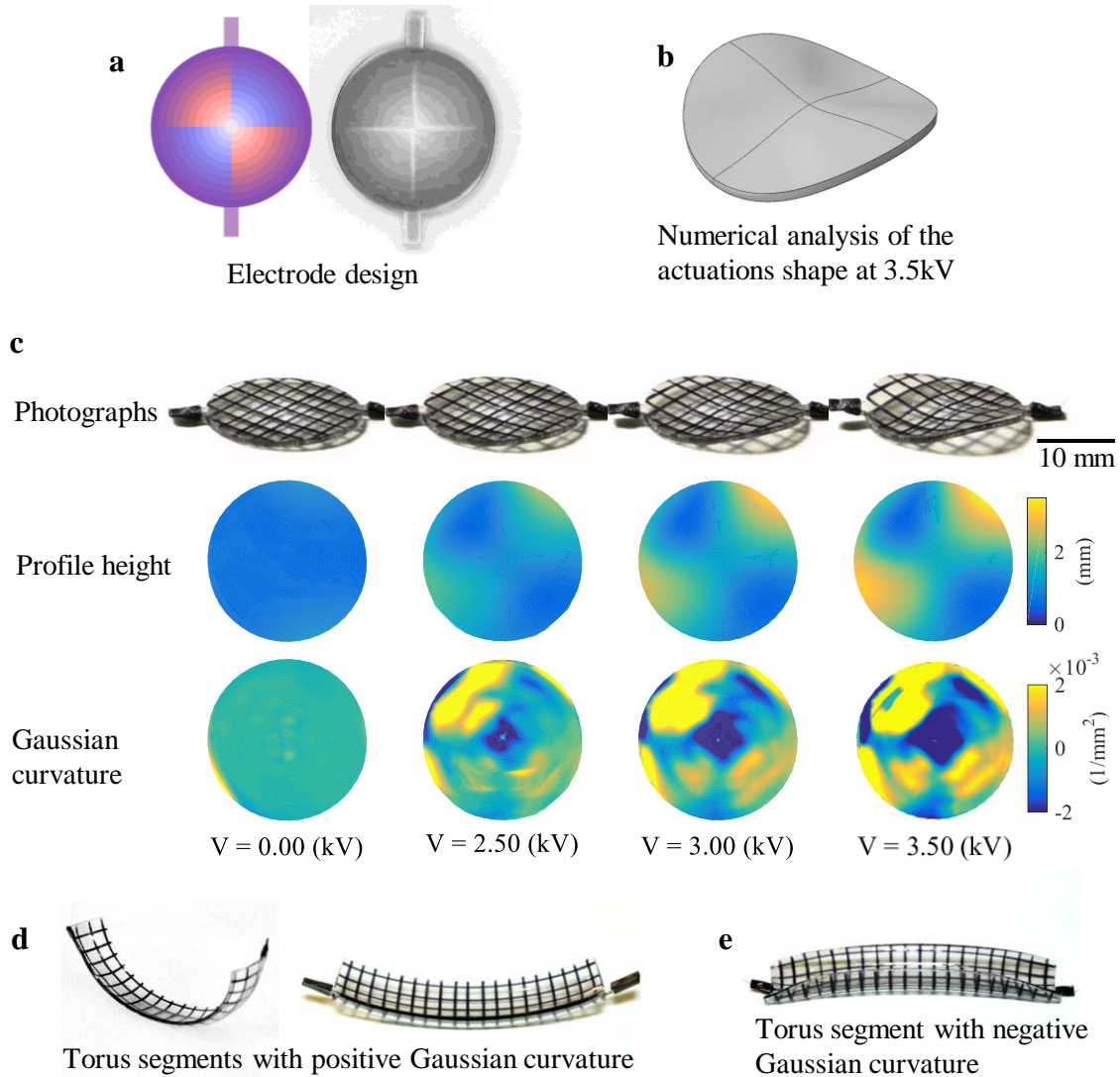


Fig. 3. A thin sheet of elastomer morphing into a saddle with negative Gaussian curvature. **(a)** The design of the electrodes to produce a negative Gaussian curvature is such that there is less electrode overlap at the center of the elastomer sheet and increasing with radius, shown schematically with the color intensity on the left. Additionally, the electrodes are designed such that the blue quadrants bend outward and the red quadrants bend inward. On the right a photograph of the elastomer sheet is shown. **(b)** Numerical analysis of this structure shows that the flat sheet of elastomer morphs into a saddle shape upon applying a voltage **(c)** A series of

photographs of the disk with increasing voltage illustrates increasing negative curvature, confirmed by the height profiles and the Gaussian curvature derived from the 3D height data. (d, e) Illustration of the generation of positive and negative curvature portions of a torus, respectively.

As shown, the multi-layering fabrication process enables a wide variety of electrode meso-architectures to be created. It also enables different sets of electrodes to be addressed and thereby produce morphing into different types of shapes according to which electrodes the voltage is applied. Furthermore, it also enables different sets of electrodes to be powered with different voltages and at different time sequences enabling different shapes to be produced. As a result of this, for instance, in Fig. 4, two sets of addressable electrodes were incorporated into the elastomer sheet. One was a set of circular electrodes, as used to create a positive Gaussian curvature, and a second set of electrodes, as used for the saddle shape were positioned on alternate layers. To fabricate an elastomer disk with this electrode meso-structure, 23 layers of elastomer sandwiched 11 electrodes for the dome and 11 electrodes for the saddle. Upon applying a voltage to the two sets of electrodes that correspond the circular disk electrodes with varying radius, the elastomer morphs into a dome shape and applying voltage to the other set of electrodes results in a saddle shape, Fig. 4. Realtime video recording of the reconfigurable actuation is shown in Supplementary Video 3.



Fig. 4. An initially flat thin circular sheet of elastomer (left) morphs into a dome shape (middle) and saddle shape (right), based on which sets of electrodes are addressed, illustrating a simple example of electrode addressable reconfigurability. The contours of reflected light highlight the local curvatures. Real time video recording of the morphing reconfigurability is shown in Supplemental Video 3.

Demonstration of the underlying concept of shape morphing in soft elastomers by manipulation of the spatial distribution of electric fields using an internal meso-architecture of electrodes lays the foundation for future device realization as well as more complex shaping. The possible shapes are fully deterministic as they depend on the three-dimensional architecture of the electrodes. Nevertheless, the reconfigurability capabilities will increase with the use of thinner elastomer sheets to increase both the density of electrodes and higher electric fields. Presently, as in other applications of dielectric elastomers, our capabilities are limited by high defect densities, non-uniformities and low dielectric breakdown strengths of currently available elastomers. Advances in multi-layering technologies for elastomers and electrodes, including higher spatial resolution electrode patterning, offer the potential to produce greater variety of reconfigurable shape morphing than illustrated in this work. In combination with an internal power supply and sensors as well as their lightweight, a variety of large displacement of motions

is possible. Finally, the ability to create complex shapes also poses a mathematical challenge, an inverse problem, of how to design the three-dimensional electrode arrangement to create specific targeted shapes.

Methods:

Precursor. The elastomer was made from an acrylic based precursor^{18,20}: 70% (by mass) of CN9018 (a urethane acrylate oligomer), 17.5% isodecyl acrylate (viscosity modifier), 5% isobornyl acrylate (toughness enhancer), 5% 1,6-hexanediol diacrylate (tunable crosslinker), 1% trimethylolpropane triacrylate (base crosslinker), 1% dimethoxy-2-phenylacetophenone and 0.5% benzophenone (a photoinitiator).

50g batches of the ingredients were added together and mixed using a planetary centrifugal mixer (Thinky Mixer ARE-310) for 20 minutes at 2000 rpm and defoamed for 30 seconds at 2200 rpm.

Fabrication. The fabrication process was similar to that used to make the multilayer dielectric elastomer actuators¹⁸: The precursor is poured onto a wafer, spin-coated for 2 minutes at 2000 rpm, and then cured for 180 seconds under ultra violet (UV) light (an array of 6 Hitachi F8T5/BL UV lamps with peak intensity at 366nm wavelength) in absence of oxygen, resulting in a 76 ± 2 μm layer of elastomer.

A mask, defining the electrode's geometry, was placed onto the elastomer sheet and a mat of carbon nanotubes pressed on it to form a compliant electrode. The mat of carbon nanotubes was formed by vacuum filtration: a suspension of carbon nanotubes (P3-SWNT, Carbon Solutions, Inc.) in deionized water with 17% transmittance at 550 nm wavelength was prepared through sonication, centrifugation and decanting²¹. 300 μL of this suspension was vacuum filtered through a porous PTFE filter membrane (0.2 μm pore and 47mm diameter, Nuclepore[®], Whatman, Florham Park, NJ), resulting in mat of carbon nanotubes on the PTFE filter membrane

with density of 6 mg/m^2 and sheet resistance of $6.7 \pm 1 \text{ k}\Omega/\square$, measured using a four-point probe sheet resistance measurement system (Keithley 6221 current source and Keithley 2182A Nanovoltmeter).

The procedure was continued by pouring the precursor onto the elastomer and repeating the spin-coating, UV curing and stamping steps for the desired number of electrodes.

Mechanical characterization. Uniaxial tension test was performed on a set of 14 dog-bone shaped specimens with the geometrical parameters suggested by ASTM D416-16 (die C scaled by half). The specimens are stretched at a constant rate of 0.1 mm/s and the tensile force was measured using a load cell (FUTEK LSB200 , 2 lb , JR S-Beam Load Cell). To measure the stretch, the distance between two marks, drawn on the narrow part of the dog-bone samples at a distance of 10 mm from each other, was measured as the specimen was stretched. The distance between these marks is measured from images recorded using a camera placed 30 cm above the sample. The measured distance over the initial distance gives the stretch. By fitting the Gent model²² to the uniaxial stress-stretch curve, the shear modulus was determined $312 \pm 8 \text{ kPa}$ and the strain hardening parameter J_{lim} was 4.3 ± 0.3 . Early strain hardening ($J_{lim} < 7$) prevents electro-mechanical instability. The stress-stretch curve and the fitted Gent model are shown Extended Data Fig. 1.

Electrical characterization. The electrical capacitance of the positive curvature actuator is measured using an LCR meter (Agilent E4980A) at 20 Hz in parallel circuit mode. The relative permittivity of the dielectric elastomer is calculated by comparing the measured capacitance to a COMSOL model of the actuator with relative permittivity of 1. Since capacitance is a linear

function of permittivity, the ratio of the measured to the simulated capacitance gives the relative permittivity.

Electrode design. The meso-architecture of the electrodes for morphing into positive and negative Gaussian curvatures is shown in Extended Data Fig. 2 and 3, respectively. To morph into a positive Gaussian curvature, the meso-architecture consists of 11 concentric, inter-digitated electrodes of decreasing radii with height, and to morph into a negative Gaussian curvature, the meso-architecture consists of 11 inter-digitated electrodes whose overlap increases linearly with radius, with the additional feature that on two opposite quadrants of the disk it increases with height while on the other two quadrants it decreases.

Profile measurement. The three-dimensional profiles of the elastomer sheets were measured using a laser line scanner (MTI ProTrak PT-G 60/40/58) and a precision linear stage (GHC SLP35, GMC Hillstone Co. and MicroFlex e100 servo drive). The line scanner was mounted to the table and the elastomer sheet was placed onto the linear stage and the voltage ramped up in steps of 100 volts. In each step, the surface of the elastomer is scanned by moving the linear stage for course of 30 mm and speed of 3 mm/s, while the voltage is constant, resulting in about 25000 points/cm² in 10 seconds.

Numerical analysis. Following the standard finite element formulation procedure ⁶, the governing partial differential equations are converted into a system of nonlinear algebraic equations. This system of nonlinear equations was then solved in Abaqus using Newton-Raphson's iterative method. An Abaqus user element (UEL) was developed to incorporate the coupling terms into the residual vector and stiffness matrix.

Actuation of dielectric elastomers is mathematically described by the balance of forces and the Gauss's flux theorem, together with a proper set of boundary conditions and constitutive equations for the material models. For quasi-static actuation, the balance of forces and Gauss's flux theorem are given by

$$\frac{\partial}{\partial x_i}(\sigma_{ij} + \sigma_{ij}^{\text{Max}}) = 0, \quad j = 1,2,3$$

$$\frac{\partial D_i}{\partial x_i} = q$$

where σ_{ij} is the Cauchy stress tensor, σ_{ij}^{Max} is the Maxwell stress tensor, D_i is electric displacement and q is the density of free charges. The two equations are coupled through the Maxwell stress tensor.

For the mechanical constitutive equation, a nearly incompressible neo-Hookean material model is adopted, which expresses the material's Helmholtz-free energy, ψ , as a function of the first and the third invariants of the Cauchy-Green deformation tensors, I_1 and I_3 :

$$\psi = \frac{\mu}{2} \left(\frac{I_1}{I_3^{1/3}} - 3 \right) + \kappa (\sqrt{I_3} - 1)^2 = \frac{\mu}{2} (\bar{I}_1 - 3) + \kappa (J - 1)^2$$

Where μ is the shear modulus and equal to 312 kPa, and κ is the bulk modulus and is set to 32.2 MPa (two orders of magnitude higher than the shear modulus to represent a nearly incompressible material). For the dielectric material model, a linear polarization constitutive equation is used, where the electric displacement D_i is a linear function of the electric field E_i :

$$D_i = \epsilon_0 \epsilon_r E_i, \quad i = 1,2,3$$

Where ϵ_0 , ϵ_r , and E are vacuum permittivity, dielectric constant of the elastomer, and the electric field inside the elastomer. The Maxwell stress for an incompressible and linearly polarizable material is related to the electric field by

$$\sigma_{ij}^{\text{Max}} = \epsilon_0 \epsilon_r \left(E_i E_j - \frac{1}{2} E_k E_k \delta_{ij} \right)$$

The two governing partial differential equations (balance of forces and Gauss's flux theorem) along with the mechanical and electrical constitutive equations and the boundary conditions describes the actuation of dielectric elastomers. Following the standard finite element formulation procedure, this system of partial differential equations is written in integral form and integrated by part. A shape function N^A is considered for the weight functions and the solution variables (displacement u_i and electric potential ϕ). The integration is performed using Gaussian quadrature. This procedure converts the set of partial differential equations into the following system of nonlinear algebraic equations:

$$\begin{Bmatrix} R_{u_j}^A \\ R_{\phi}^A \end{Bmatrix} = \begin{Bmatrix} - \sum_{n_G} (\sigma_{ij} + \sigma_{ij}^{\text{Max}}) \frac{\partial N^A}{\partial x_i} w_{n_G} \det \frac{\partial x_p}{\partial \xi_q} + \sum_{n_G} (t_j N^A) w_{n_G} \det \frac{\partial x_p}{\partial \xi_q} \\ - \sum_{n_G} \left(D_i \frac{\partial N^A}{\partial x_i} + q N^A \right) w_{n_G} \det \frac{\partial x_p}{\partial \xi_q} + \sum_{n_G} (q_s N^A) w_{n_G} \det \frac{\partial x_p}{\partial \xi_q} \end{Bmatrix} = \begin{Bmatrix} 0 \\ 0 \end{Bmatrix}$$

For $j = 1, 2, 3$ and $A = 1, \dots, N$, (N being the total number of the nodes). These nonlinear algebraic equations were solved iteratively using Newton-Raphson's method:

$$\begin{Bmatrix} R_{u_j}^A \\ R_{\phi}^A \end{Bmatrix}^{i+1} = \begin{Bmatrix} R_{u_j}^A \\ R_{\phi}^A \end{Bmatrix}^i + \frac{\partial}{\partial u_k^B} \begin{Bmatrix} R_{u_j}^A \\ R_{\phi}^A \end{Bmatrix}^i \delta u_k^B + \frac{\partial}{\partial \phi^B} \begin{Bmatrix} R_{u_j}^A \\ R_{\phi}^A \end{Bmatrix}^i \delta \phi^B = \begin{Bmatrix} 0 \\ 0 \end{Bmatrix}, \quad j = 1, 2, 3, \quad A = 1, \dots, N$$

Where the superscripts $i + 1$ and i are the iteration number. In each iteration, the following linear algebraic equations need to be solved:

$$\begin{bmatrix} K_{u_j^A u_k^B} & K_{u_j^A \phi^B} \\ K_{\phi^A u_k^B} & K_{\phi^A \phi^B} \end{bmatrix} \begin{Bmatrix} \delta u_k^B \\ \delta \phi^B \end{Bmatrix} = \begin{Bmatrix} R_{u_j}^A \\ R_{\phi}^A \end{Bmatrix}, \quad j = 1, 2, 3, \quad A = 1, \dots, N$$

The solution variables u_k^B and ϕ^B are obtained through iteratively solving this system of linear algebraic equations until the residual vector and change of the solution variables are within the convergence criterion.

Abaqus/CAE is implemented to define the geometry and the boundary conditions, mesh the geometry, assemble the element stiffness matrices and the residual vectors, solve the system of algebraic equations through Newton-Raphson's method, and visualize the results. An Abaqus user element (UEL) is developed to incorporate the coupling terms $K_{u_j^A \phi^B}$ and $K_{\phi^A u_k^B}$ into the element stiffness matrix, and the Maxwell stress term into the element residual vector.

Data availability. All data generated or analysed during this study are included in the published article and its Supplementary information and are available from the corresponding author on reasonable request.

References:

- 1 Liang, H. & Mahadevan, L. The shape of a long leaf. *Proceedings of the National Academy of Sciences* **106**, 22049-22054 (2009).
- 2 Bayly, P., Taber, L. & Kroenke, C. Mechanical forces in cerebral cortical folding: a review of measurements and models. *Journal of the mechanical behavior of biomedical materials* **29**, 568-581 (2014).
- 3 Nath, U., Crawford, B. C., Carpenter, R. & Coen, E. Genetic control of surface curvature. *Science* **299**, 1404-1407 (2003).
- 4 Klein, Y., Efrati, E. & Sharon, E. Shaping of elastic sheets by prescription of non-Euclidean metrics. *Science* **315**, 1116-1120 (2007).
- 5 Holmes, D. P., Roché, M., Sinha, T. & Stone, H. A. Bending and twisting of soft materials by non-homogenous swelling. *Soft Matter* **7**, 5188-5193 (2011).
- 6 Pezzulla, M., Shillig, S. A., Nardinocchi, P. & Holmes, D. P. Morphing of geometric composites via residual swelling. *Soft Matter* **11**, 5812-5820 (2015).
- 7 Egunov, A., Korvink, J. & Luchnikov, V. Polydimethylsiloxane bilayer films with an embedded spontaneous curvature. *Soft matter* **12**, 45-52 (2016).
- 8 Gladman, A. S., Matsumoto, E. A., Nuzzo, R. G., Mahadevan, L. & Lewis, J. A. Biomimetic 4D printing. *Nature materials* **15**, 413 (2016).
- 9 Kim, J., Hanna, J. A., Byun, M., Santangelo, C. D. & Hayward, R. C. Designing responsive buckled surfaces by halftone gel lithography. *Science* **335**, 1201-1205 (2012).
- 10 Kim, J., Hanna, J. A., Hayward, R. C. & Santangelo, C. D. Thermally responsive rolling of thin gel strips with discrete variations in swelling. *Soft Matter* **8**, 2375-2381 (2012).
- 11 Pikul, J. *et al.* Stretchable surfaces with programmable 3D texture morphing for synthetic camouflaging skins. *Science* **358**, 210-214 (2017).
- 12 Kim, Y., Yuk, H., Zhao, R., Chester, S. A. & Zhao, X. Printing ferromagnetic domains for untethered fast-transforming soft materials. *Nature* **558**, 274 (2018).
- 13 Pelrine, R., Kornbluh, R., Pei, Q. & Joseph, J. High-speed electrically actuated elastomers with strain greater than 100%. *Science* **287**, 836-839 (2000).
- 14 Carpi, F. & De Rossi, D. Dielectric elastomer cylindrical actuators: electromechanical modelling and experimental evaluation. *Materials Science and Engineering: C* **24**, 555-562 (2004).
- 15 Carpi, F., Salaris, C. & De Rossi, D. Folded dielectric elastomer actuators. *Smart Materials and Structures* **16**, S300 (2007).
- 16 Shian, S., Bertoldi, K. & Clarke, D. R. Dielectric elastomer based “grippers” for soft robotics. *Advanced Materials* **27**, 6814-6819 (2015).
- 17 Ciarlet, P. G. An introduction to differential geometry with applications to elasticity. *Journal of Elasticity* **78**, 1-215 (2005).
- 18 Duduta, M., Wood, R. J. & Clarke, D. R. Multilayer dielectric elastomers for fast, programmable actuation without prestretch. *Advanced Materials* **28**, 8058-8063 (2016).
- 19 Yeoh, O. Some forms of the strain energy function for rubber. *Rubber Chemistry and technology* **66**, 754-771 (1993).

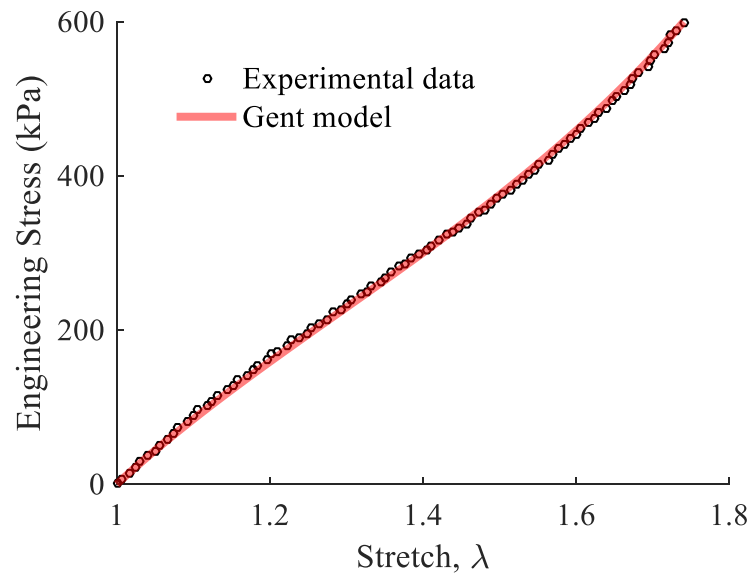
- 20 Niu, X. *et al.* Synthesizing a new dielectric elastomer exhibiting large actuation strain and suppressed electromechanical instability without prestretching. *Journal of Polymer Science Part B: Polymer Physics* **51**, 197-206 (2013).
- 21 Shian, S., Diebold, R. M., McNamara, A. & Clarke, D. R. Highly compliant transparent electrodes. *Applied Physics Letters* **101**, 061101 (2012).
- 22 Gent, A. A new constitutive relation for rubber. *Rubber chemistry and technology* **69**, 59-61 (1996).

Acknowledgments: This work was supported by the MRSEC through the National Science Foundation grant DMR 14-20570. The authors are grateful to Mihai Duduta for his helpful comments and his assistance with preparing the materials.

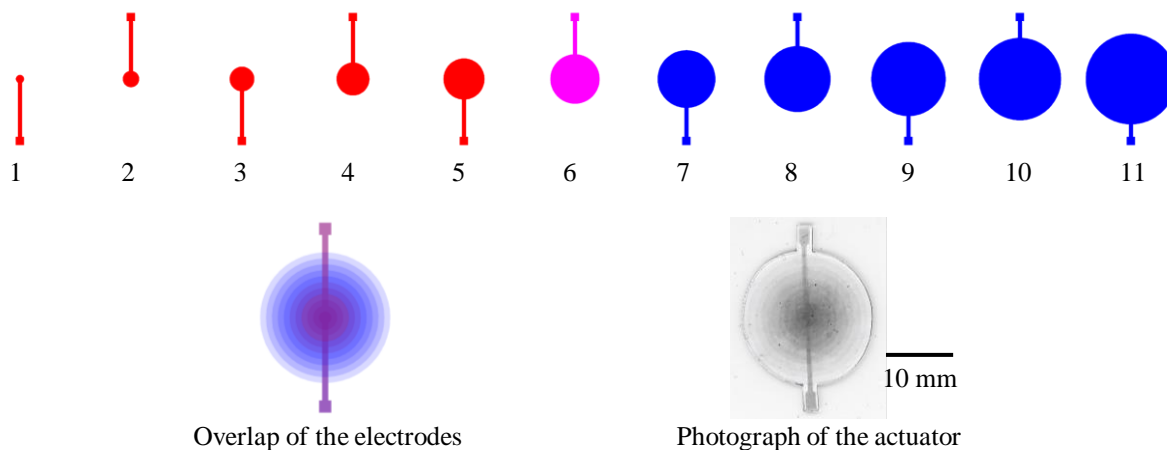
Author contributions: D.R.C. conceived and supervised the project. E.H. performed the experiments and the numerical calculations. Both authors contributed to the writing of the manuscript.

Competing interests: The authors declare no competing interests.

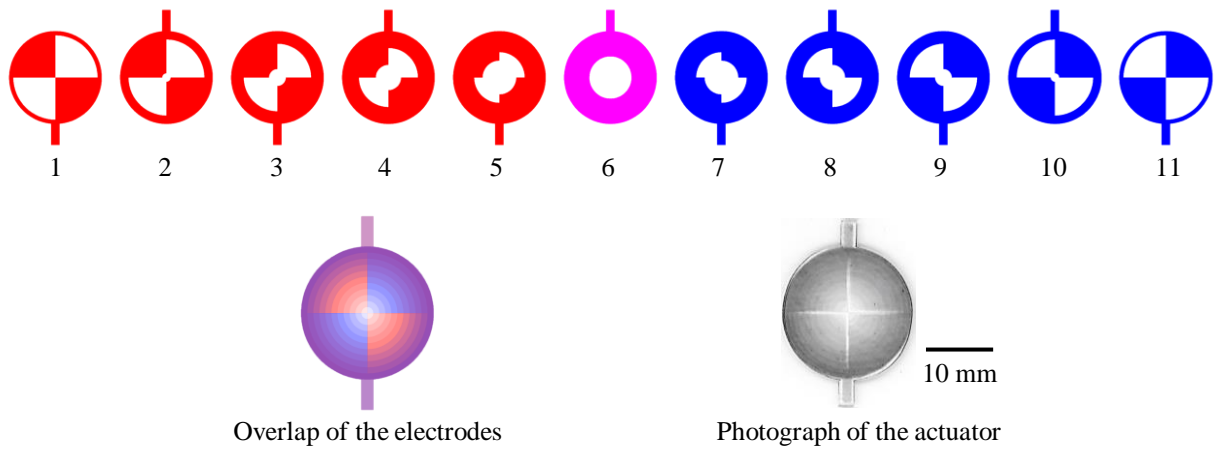
Materials & Correspondence: Correspondence and requests for materials should be addressed to D.R.C. (email: clarke@seas.harvard.edu)



Extended Data Fig. 1. Uniaxial stress-stretch curve of the elastomer and the fitted Gent model.



Extended Data Fig 2. To morph a flat sheet of dielectric elastomer to a positive Gaussian curvature, the meso-architecture of the electrodes consists of 11 concentric, inter-digitated electrodes of decreasing radii with height. As a result, the overlap of the electrodes increases linearly with radius. The electrodes below the mid-surface (electrodes 1-5) and above the mid-surface (electrodes 7-11) are represented by red and blue, respectively.



Extended Data Fig 3. To morph a flat sheet of dielectric elastomer to a negative Gaussian curvature, the meso-architecture of the electrodes consists of 11 inter-digited electrodes whose overlap increases linearly with radius, with the additional feature that on two opposite quadrants of the disk it increases with height while on the other two quadrants it decreases. The electrodes below the mid-surface (electrodes 1-5) and above the mid-surface (electrodes 7-11) are represented by red and blue, respectively.